Eur. Phys. J. D **2**, 217–230 (1998)

THE EUROPEAN PHYSICAL JOURNAL D

The two-photon 2s → 1s transition of the fully-ionized muonic boron migrating in helium

S.V. Romanov[a]

Department 52 (O-52) Institute of General and Nuclear Physics, Russian Research Centre "Kurchatov Institute", 123 182 Moscow, Russia

Received: 21 October 1997 / Revised: 16 January 1998 / Accepted: 2 March 1998

Abstract. In recent experiments performed at the Paul Scherrer Institute (PSI) measurements were made of the yield $Y_{2\gamma}$ of the two-photon $2s \to 1s$ transition of the fully-ionized muonic boron formed and quenched in a gaseous mixture of diborane B_2H_6 and helium. In the present work this yield is calculated for an idealized case of a very low diborane density when the main $2s$ state decay modes competing with the two-photon transition are due to the electron transfer from helium to the μ-ion. As the rate of this transfer depends strongly on the relative velocity, a treatment is needed of the whole kinetics of processes occurring with the μ-ion in helium. Accordingly, within the optical model with a complex potential constructed before we calculate cross-sections of the elastic scattering and electron transfer. Then the time evolution of the μ-ion energy is considered and, finally, the yield $Y_{2\gamma}$ is calculated. It proves that at helium pressures $P_{\rm He} \geq 50$ Torr this yield may be written in the form: $(Y_{2\gamma})^{-1} = C(1 + P_{\rm He}D)$, where the factor C is greater than unity and increases rapidly with the initial energy E_0 which the μ-ion has after its formation in the diborane molecule. Thus measurement of the pressure dependence of $Y_{2\gamma}$ allows E_0 to be estimated. The results obtained make it possible to suggest a similar parametrization of the PSI data.

PACS. 34.50.Bw Energy loss and stopping power – 34.70.+e Charge transfer – 36.10.Dr Positronium, muonium, muonic atoms and molecules

1 Introduction

The discovery of weak neutral currents in 1973 stimulated a search for ways of their detection in various physical systems. One of the original proposals concerned effects caused by the weak neutral current interaction of the negative muon and a nucleus in light muonic atoms. The idea consisted of the following [1–3]. Let a μ-atom be in its $2s$ state. Its energy is close to that of the $2p$ state of opposite parity. The parity-violating part of the weak interaction leads to the $2s$ state acquiring an admixture of the $2p$ state. As a result, the amplitude of the one-photon $2s \to 1s$ transition of the muon becomes a sum of magnetic and electric dipole amplitudes. Their interference leads to the appearance of a number of observable P-odd correlations. For instance, if the muon spin in the $2s$ state is polarized, the angular photon distribution becomes asymmetrical. It includes a term proportional to the first Legendre polynomial. If the muon spin is unpolarized, a nonvanishing circular polarization of the photon arises. Moreover, the muon spin polarization in the final $1s$ state proves to be nonzero and leads to a correlation of the momenta directions of the photon and the hard electron from the subsequent μ-decay at the $1s$ orbit [4,5]. In principle, measurements of these correlations make it possible to determine constants of the weak neutral current interaction [4–8].

The P-odd correlations can be rather large. They amount to several per cent in μ-atoms of the region $2 \leq Z \leq 5$ (Z is the atomic number). Nevertheless, experiments on their observation have not yet been performed. The reason is that the one-photon $2s \to 1s$ transition is strongly forbidden in light μ-atoms and is very difficult for detection. Even in the most favourable, idealized situation of a fully-ionized μ-atom isolated from an external influence the relative yield of this transition per one muon in the $2s$ state is very small–about 10^{-6} for muonic helium and 10^{-4} for muonic boron [1–5,9]. The actual situation is much worse. This is connected with the μ-atoms with $Z \geq 2$ being able to hold several bound electrons. Some of them may remain after the atomic muon cascade to the $2s$ state, others may be intercepted from surrounding atoms or molecules during the $2s$ state lifetime. The presence of bound electrons opens additional, very intensive channels of the $2s$ state decay [10–13]. As a result, the yield of the one-photon transition falls additionally by several orders of magnitude. Moreover, in some of these channels there is an intense radiation whose energy is close to that of the $2s \to 1s$ transition. The background resulting from this radiation is a serious obstacle to a detection of the

[a] e-mail: roman@cerber.polyn.kiae.su

one-photon transition. There are also other reasons for the appearance of such a background. In muonic hydrogen which can not hold electrons it is due to the well-known process of the radiative quenching of the $2s$ state in collisions with hydrogen molecules [14–16]. This process is also significant for muonic helium but becomes less important for heavier μ-atoms [4].

The previous consideration shows that the one-photon $2s \to 1s$ transition may be observed provided the μ-atom is formed in a rarefied gas. In this case one may hope to suppress both the electron transfer from gas molecules to the μ-atom and the radiative collisional quenching of the $2s$ state. However, a serious problem arising here is to provide a sufficient muon stop density. A way of solving this was found at the Paul Scherrer Institute (Switzerland) where the cyclotron trap was put into operation [17]. This made it possible to begin preliminary experiments searching for the conditions necessary for observing the P-odd correlations in muonic boron. The reasons why just this μ-atom was chosen are presented in [5]. The first step [18] was to a obtain the fully-ionized muonic boron in the $2s$ state and to prevent the electron transfer during its lifetime. In this case the $2s$ state is metastable. Its lifetime is about 32 ns [9] and its main decay mode is the two-photon $2s \to 1s$ transition. Thus, the presence of two-photon events in an experiment may be an indicator of the $2s$ state metastability. The experiment [18] was devoted to a search of such events in a mixture of a small amount of diborane gas (B_2H_6) with helium. The mixture was at room temperature, its pressure was varied from 20 to 165 Torr, the diborane concentration – from 0.3 to 5%. The important point was the use of helium as a moderator of muons injected into the trap. This made it possible to reduce the partial diborane pressure to a few decitorr and, as a result, to suppress the electron transfer to a maximum degree because it is natural to expect that the electron transfer in collisions of muonic boron with helium is considerably less effective than in collisions with diborane. The experiment proved to be successful. Two-photon events were actually observed at some combinations of the helium pressure and diborane percentage. Besides being important for planning an experiment on measuring the P-odd correlations this result may be of interest for physics of atomic processes. Just this aspect is discussed in the present paper.

In [18] the relative yield of the two-photon transition per one muon in the $2s$ state was extracted from experimental data and parametrized as follows:

$$Y_{2\gamma} = \lambda_{2\gamma} / \left(\lambda_{2\gamma} + \rho_{\mathrm{He}} q_{\mathrm{He}} + \rho_{\mathrm{B_2H_6}} q_{\mathrm{B_2H_6}}\right). \qquad (1)$$

$\lambda_{2\gamma} = 3.09 \times 10^7\ \mathrm{s}^{-1}$ is the two-photon transition rate in the isolated muonic boron [9], ρ_{He} and $\rho_{\mathrm{B_2H_6}}$ are the helium and diborane densities (in cm^{-3}), q_{He} and $q_{\mathrm{B_2H_6}}$ are some effective rate constants of the electron transfer from helium and diborane. The denominator of (1) is treated as the total decay rate of the $2s$ state in the gaseous mixture. The following values of the rate constants were found:

$$q_{\mathrm{He}} = (0.10 \pm 0.18) \times 10^{-10}\ \mathrm{cm}^3\ \mathrm{s}^{-1}, \qquad (2)$$

$$q_{\mathrm{B_2H_6}} = (0.55 \pm 0.22) \times 10^{-8}\ \mathrm{cm}^3\ \mathrm{s}^{-1}. \qquad (3)$$

Only the upper limit on q_{He} was actually placed. It is less than $q_{\mathrm{B_2H_6}}$ by, at least, two orders of magnitude. This result confirms the correctness of the above-mentioned idea to reduce the partial diborane pressure by introducing helium as a moderator. Nevertheless, in spite of rather small values of this pressure achieved in the experiment the electron transfer to muonic boron was mainly due to collisions with diborane molecules.

Let us take the following physical picture of the muonic boron formation and its subsequent behaviour in the gaseous mixture. Muons injected into the trap are slowed down by collisions with helium atoms. After their energy has reached suitable values, they start to be captured by diborane molecules. The next stage is the cascade of Auger and radiative transitions of the muon occurring in the molecule and leading, in particular, to the formation of the fully-ionized μ-atom in the $2s$ state. For the subsequent consideration, it will be important to know typical kinetic energies acquired by the μ-atom during its formation. As the atomic capture and cascade occur in the complex molecule, estimations of these energies are very uncertain. For instance, the simplest assumption is that the μ-atom acceleration is due to the energy transfer in the atomic capture as well as the recoil in cascade transitions. In this case the resulting kinetic energy of muonic boron proves to be about 1 eV or less (the muon energy before the atomic capture is taken to be less than 100 eV). However, that the μ-atom is formed in the molecule may lead to its additional acceleration. Indeed, the molecule is destroyed during the Auger cascade. As a result, positively charged molecular fragments may appear together with the ionized μ-atom. Because of their mutual repulsion they start to fly apart. During this process the μ-atom may acquire an additional gain in energy, the scale of which is determined by a typical energy of the repulsion. Its crude estimation is obtained within the assumptions that the molecular fragments are singly or doubly charged, and effective distances between them are equal to several Angström. In this case the μ-atom energy proves to be of the order of one atomic unit (1 a.u. = 27.2 eV).

After the fully-ionized μ-atom in the $2s$ state has been formed, it starts to migrate in the gas by colliding with helium atoms and diborane molecules. Collisions destroy the $2s$ state metastability and reduce the yield of the two-photon transition. For instance, the μ-atom can intercept an electron in a collision. This causes a fast quenching of the $2s$ state by decay modes connected with an excitation of the bound electron or its ejection in the continuum [10, 11]. It is clear that the results (1-3) carry information on collisions in which the μ-atom takes part, as well as on the stage of its formation in the diborane molecule. This stage determines the initial kinetic energy with which the μ-atom starts to migrate in the gas and which is manifested due to the energy dependence of collision rates. An attempt to extract such information was made in [19] where the electron transfer from helium to the μ-atom was considered. As the radius of $(\mu\mathrm{B})^{4+}$ is much less than radii of electron orbits, the μ-atom was treated as a heavy

beryllium isotope Be^{4+} (a point, quadruply charged nucleus with the μ-atom mass). It was found that the main reaction responsible for the electron transfer was:

$$Be^{4+} + He \to Be^{3+}(1s) + He^{2+} + e^-. \qquad (4)$$

The final state involves the one-electron ion $Be^{3+}(1s)$ in its ground state, the helium nucleus He^{2+} and one unbound electron. This reaction results from the Auger effect in the two-electron quasi-molecule $(Be{-}He)^{4+}$. Its total cross-section σ_A was calculated within the following approximations. The nuclei Be^{4+} and He^{2+} interact by forces whose potential is determined by the electronic quasi-molecule state correlated to the entrance channel Be^{4+} + He in the separated atoms limit. At any finite internuclear distance this state is autoionized and can decay due to the Auger transition to the ground electronic state of the one-electron quasi-molecule $(Be{-}He)^{5+}$. This system is unbonded and decays into $Be^{3+}(1s)$ and He^{2+}. The interaction potential was calculated by diagonalizing the electronic Hamiltonian of $(Be{-}He)^{4+}$ on a basis of several diabatic states constructed from two-centre orbitals. The electronic wavefunction built in this way was used to calculate the Auger transition rate. The Auger electron was described by a plane wave. The relative motion of the nuclei was considered to be in classical paths. The collision energy T was varied from 10^{-3} to several atomic units. Its lower limit corresponds to the thermal energy (1/40 eV). At 10^{-3} a.u. $\leq T \leq 10^{-2}$ a.u. the cross-section σ_A was found to be small ($\sim 10^{-2}$ Å^2) and to decrease inversely with the relative velocity v. At higher collision energies it increases fast, amounting to typical atomic values of 1 Å^2 at $T = 1{-}2$ a.u., and then remains nearly at this level. The comparison of values of the product $(v\sigma_A)$ with the experimental result (2) made it possible to place an upper limit on the energy of collisions in which the μ-atom takes part during the $2s$ state lifetime (32 ns). It proved to be about 0.3 a.u. The corresponding μ-atom energy in the laboratory frame is greater by a factor of 3.5, and is about 1 a.u. This limit agrees with the assumption that the energy of the μ-atom after its formation in the diborane molecule is about 1 eV and results from the energy transfer in the atomic muon capture and the recoil in cascade transitions. However, it does not exclude the possibility of the additional acceleration of the μ-atom caused by its Coulomb repulsion from positively charged molecular fragments. Unfortunately, the large errors in (2) do not allow the latter mechanism to be indicated with certainly. The result (3) is more definite, but unlikely to yield something because a realistic calculation of the electron transfer from diborane to the μ-atom seems to be impossible at present. It should be emphasized that the above-mentioned estimation of the μ-atom energy is very crude because it is based on the relation $q_{He} \equiv v\sigma_A$. Actually this is not correct. A calculation of q_{He} is a complicated problem involving the solution of a time-dependent kinetic equation for a distribution function of μ-atoms migrating in the gas.

In connection with the presented results it is of interest to find out what, in principle, can be obtained from measurements of the two-photon transition yield. Accordingly, in this paper we consider this question for an idealized case in which the fully-ionized muonic boron in its $2s$ state is formed in the mixture of He and B_2H_6, but the pressure of diborane is so small that its contribution to the electron transfer is negligible. This means the validity of the following inequality in (1):

$$\rho_{B_2H_6} q_{B_2H_6} \ll \rho_{He} q_{He}. \qquad (5)$$

A detection of the two-photon transition under such conditions seems to be impossible now because of a too low density of μ-atoms. However, this is the clearest case for a theoretical consideration and it is natural to begin with it. In Section 2 we calculate the differential cross-section of the elastic scattering of $(\mu B)^{4+}$ by helium as well as supplement the calculation of σ_A made in [19]. In Section 3 these cross-sections are used to write a kinetic equation for a distribution function of migrating μ-atoms. Its approximate solution is found and used to obtain the two-photon transition yield as a function of the helium pressure. Conclusions are cited in the same section. If it is not indicated specifically, atomic units are used everywhere.

2 The elastic and inelastic scattering of $(\mu B)^{4+}$ by helium

In the present consideration $(\mu B)^{4+}$ is also treated as a heavy beryllium isotope Be^{4+}. In accordance with [19] at the relevant collision energies the two-electron quasi-molecule $(Be{-}He)^{4+}$ may be considered to be in its autoionized electronic state correlated to the entrance channel Be^{4+} + He in the separated atoms limit. The Auger decay of this state during the collision results in the reaction (4). Such a situation may be phenomenologically described by the Schrodinger equation with a complex potential [20]. In our case this potential is:

$$V(r) = U(r) - iW(r)/2. \qquad (6)$$

r is the internuclear distance, $U(r)$ is the potential of forces by which the nuclei Be^{4+} and He^{2+} interact in the quasi-molecule, $W(r)$ is the Auger decay rate. $V(r)$ represents the electronic energy of the quasi-molecule in the adiabatic approximation (with addition of the Coulomb nuclear repulsion). Its second term leads to the usual decay factor $\exp(-W(r)t)$ in the electronic density. We use $U(r)$ and $W(r)$ calculated in [19], but $U(r)$ is defined more accurately near its zero at $r \approx 4.5$ because this part of $U(r)$ is significant in calculating the cross-section of (4) at thermal energies. The plots of $U(r)$ and $W(r)$ are shown in Figure 1. At small distances $U(r)$ is determined by the repulsion of Be^{4+} and He^{2+}:

$$U(r \to 0) = 8/r. \qquad (7)$$

At intermediate r there is a potential well, and at large distances $U(r)$ is due to the long-range attraction of Be^{4+} and He:

$$U(r \to \infty) = -8\beta/r^4. \qquad (8)$$

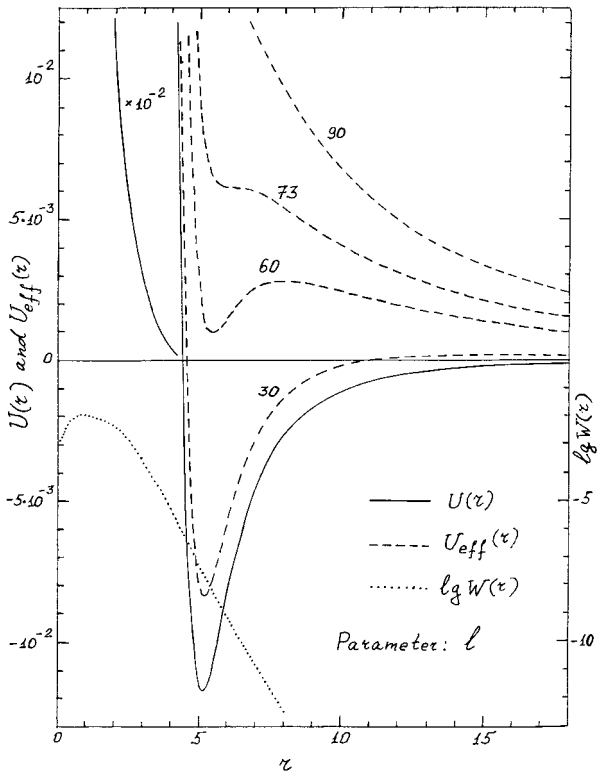

Fig. 1. The potentials U and U_{eff} (left ordinates) as well as the Auger decay rate W (right ordinates) *versus* the internuclear distance r. At $r \leq 4$, $U(r)$ is shown multiplied by 10^{-2}.

$\beta = 1.383$ is the dipolar polarizability of helium [21]. An important consequence of this attraction is a hump of curves of the effective potential (Fig. 1):

$$U_{eff}(r) = U(r) + \frac{l(l+1)}{2m\ r^2}\,. \tag{9}$$

l is the orbital angular momentum of the nuclei about their center of mass, m is the reduced mass. Because of the repulsive branch of $U(r)$ the hump exists only at $l \leq 72$. If the collision energy T becomes less than the hump height, the nuclei can not reach the potential well in classical paths. This leads, in particular, to a considerable suppression of the Auger effect because its rate $W(r)$ is seen from Figure 1 to decrease exponentially at large r.

The subsequent procedure is standard [20]. It is reduced to a calculation of complex phase shifts:

$$\eta_l = \delta_l + i\mu_l. \tag{10}$$

The set of η_l specifies the relevant cross-sections completely. The elastic differential cross-section is:

$$d\sigma_{el}/d\Omega = |f(\vartheta)|^2, \tag{11}$$

$d\Omega = 2\pi \sin\vartheta\ d\vartheta$, ϑ is the scattering angle in the center-of-mass frame, $f(\vartheta)$ is the scattering amplitude:

$$f(\vartheta) = (1/2ik)\sum_{l=0}^{\infty}(2l+1)[\exp(2i\eta_l) - 1]P_l(\cos\vartheta), \tag{12}$$

$$k = (2mT)^{1/2}, \tag{13}$$

$P_l(\cos\vartheta)$ is the Legendre polynomial. The total elastic cross-section is:

$$\sigma_{el} = (2\pi/k^2)\sum_{l=0}^{\infty}(2l+1)(\mathrm{ch}2\mu_l - \cos 2\delta_l)\exp(-2\mu_l). \tag{14}$$

The total cross-section of the reaction (4) is:

$$\sigma_A = (\pi/k^2)\sum_{l=0}^{\infty}(2l+1)Q_l, \tag{15}$$

$$Q_l = 1 - \exp(-4\mu_l). \tag{16}$$

Q_l may be treated as the Auger effect probability in the collision with the given T and l. In [19] it was calculated by considering the relative motion of the nuclei to be in classical paths.

The phase shifts are calculated by a numerical integration of the Schrodinger equation for the complex radial function [20]. The Numerov method is used [22]. The integration is undertaken out outwards from the origin untill the internuclear distance r finds itself in the asymptotic region where $U(r)$ may be well approximated by (8) and $W(r)$ is negligible. It is known that for long-lange potentials similar to (8) special care should be taken to stop the numerical integration as soon as possible and, thereby, to reduce computation time and to prevent an accumulation of errors. Accordingly, on the basis of ideas formulated in [22], we construct two linearly independent solutions of the radial equation in the asymptotic region. The radial function is their linear combination with coefficients which are found by its join with the function obtained by the numerical integration at smaller r. μ_l and δ_l are expressed in terms of these coefficients: μ_l-unambigously, while δ_l-with an accuracy to an integer multiple of π. We write it as follows:

$$\delta_l = \nu_l + N\pi. \tag{17}$$

ν_l is defined so that $|\nu_l| \leq \pi/2$, and the integer N is:

$$N = \lim_{R\to\infty}[n(R) - n_{\mathrm{B}}(R)]. \tag{18}$$

$n(R)$ and $n_{\mathrm{B}}(R)$ are the numbers of zeroes of, respectively, the real part of the complex radial function and the Bessel function $J_{l+1/2}(kr)$ within the interval $0 \leq r \leq R$. If $R \to \infty$, both $n(R)$ and $n_{\mathrm{B}}(R)$ become infinite, but their difference remains finite. It indicates just how strongly the potential distorts the wave function. The form (17) is very natural in the limit $W(r) \equiv 0$ (potential nonreactive scattering). Our case is rather close to this limit because the Auger effect probabilities Q_l are small at the relevant energies [19].

To illustrate the results obtained we present some plots of δ_l *vs.* l made for different collision energies (Figs. 2 and 3). Classical deflection functions θ_l calculated for

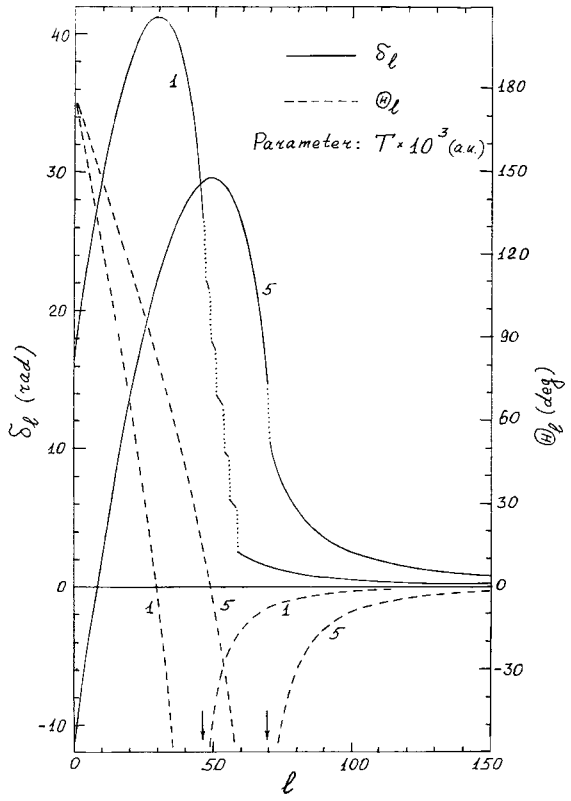

Fig. 2. The real part δ_l of the complex phase shift (left ordinates) and the classical deflection function θ_l (right ordinates) *versus* the angular momentum l for the spiral scattering. The dotted lines indicate discontinuities of δ_l curves. The vertical arrows indicate positions of the orbiting singularity of θ_l.

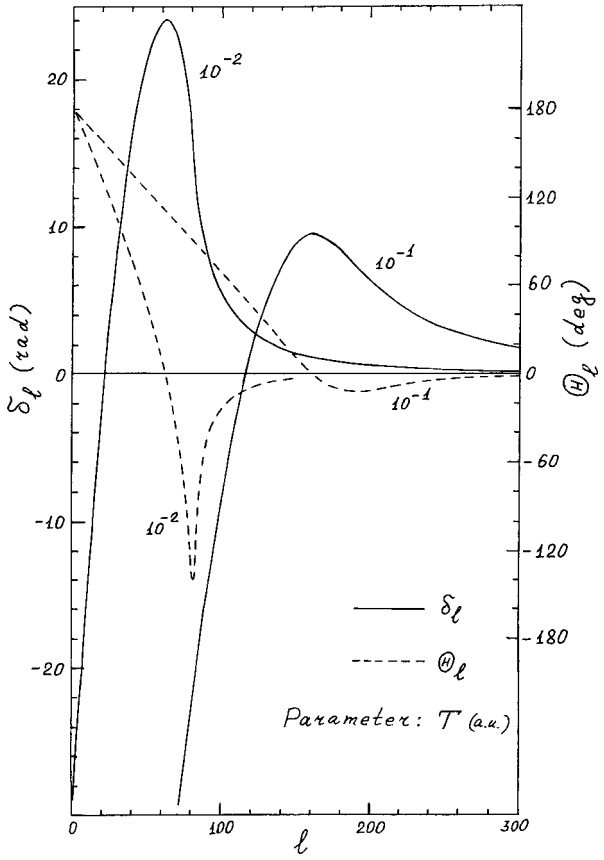

Fig. 3. The real part δ_l of the complex phase shift and the classical deflection function θ_l *versus* the angular momentum l for the rainbow scattering.

the potential $U(r)$ with the standard formulae [20] are also shown. Curves of δ_l demonstrate a number of features peculiar to the potential ion-atom scattering under quasiclassical conditions [20,23]. At first δ_l increases with l, mounts to its maximum and starts to decrease. At low energies this decrease involves a few discontinuous jumps (Fig. 2), the reason for which is that starting from some l the collision energy becomes less than the height of a hump in the effective potential. In this case the classical deflection function has a logarithmic singularity which is known to be connected with the orbiting phenomenon. After the region of jumps a curve of δ_l becomes nearer and nearer to that obtained within the Born approximation for the polarization potential (8). At large l it follows the formula [20]:

$$\delta_l = 2\pi\beta m k^2 / l^3 \tag{19}$$

As the collision energy is increased, it becomes greater than the height of any potential hump, and the jumps of δ_l disappear (Fig. 3). The singularity of the deflection function is replaced by a finite minimum. Because of a growing effect of the repulsive branch of $U(r)$ this minimum becomes shallower and broader. For the same reason curves of δ_l are transformed so that the region of negative δ_l becomes more and more appreciable. One should note that in a rather wide interval of collision energies and angular momenta our values of δ_l agree well with those calculated within the WKB approximation [20]. In this case the classical equivalence relation $\theta_l = 2\partial\delta_l/\partial l$ is satisfied with a good accuracy. However, the WKB method becomes inapplicable as the collision energy approaches the top of a potential hump. The numerical integration of the Schrodinger equation is needed in this case. Concerning l-dependences of the Auger effect probability Q_l (Fig. 4), they are similar to those obtained in [19]. A certain increase of Q_l at low collision energies is due to the already-mentioned, more accurate definition of $U(r)$ near its zero. Q_l is seen to fall abruptly starting from some l. This results from the Auger decay rate $W(r)$ decreasing exponentially at large r where paths with high l lie. Actually this fall of Q_l places a finite upper limit in the sum (15). It should be noted that the classical consideration of the relative motion used in [19] predicts an increase of Q_l as the collision energy approaches the top of a potential hump. As the classical mechanics is obviously inapplicable in this case, such an increase is nonphysical and it was ignored in [19]. The correctness of this judgement is confirmed by the present quantum-mechanical treatment which shows no increase of Q_l near the hump top. Instead, it indicates a possibility of a considerable increase of Q_l at energies less than the hump height. This is connected with

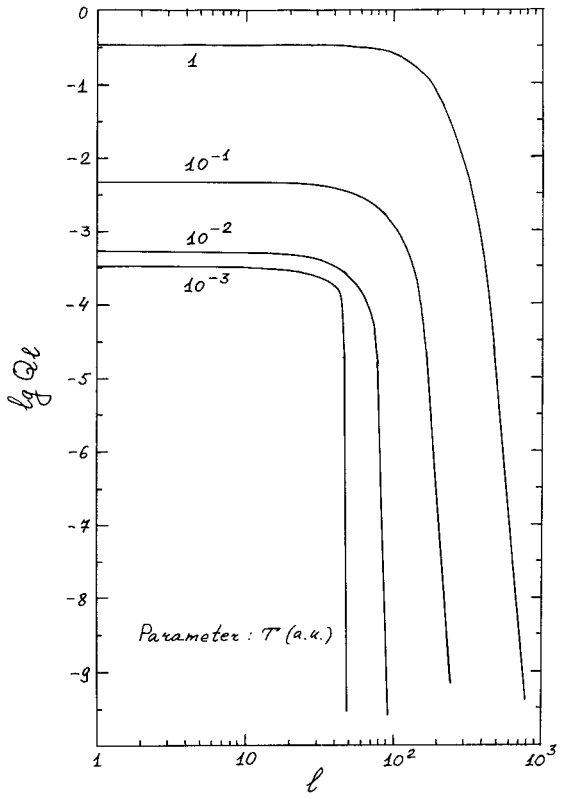

Fig. 4. The partial probabilities of the Auger effect Q_l *versus* the angular momentum l.

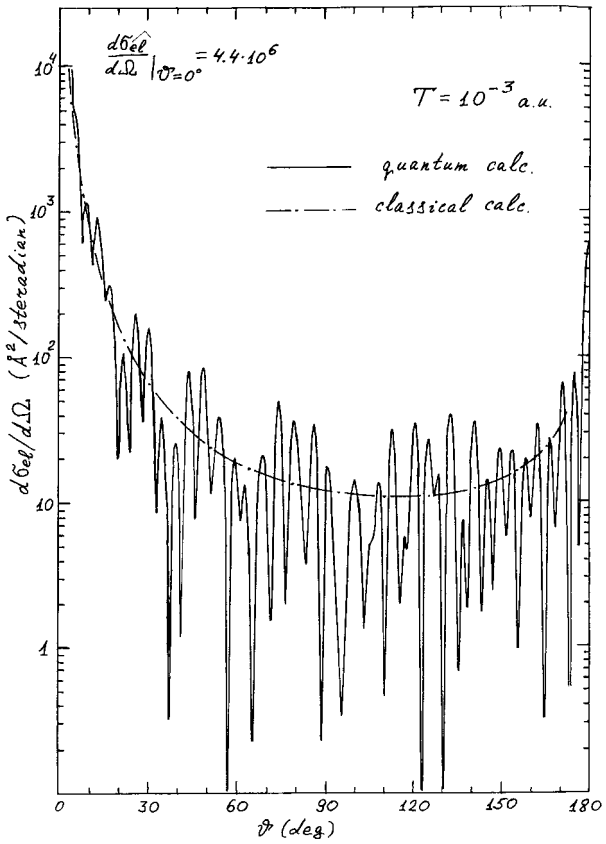

Fig. 5. The elastic differential cross-section *versus* the center-of-mass scattering angle for the spiral scattering at $T = 10^{-3}$.

the existence of quasisteady states in the effective potential. Within a narrow energy interval the wave function of such a state penetrates effectively into the classically allowed region of the internal potential well. As the Auger decay rate $W(r)$ increases fast as r is decreased, this leads to the appearance of a sharp peak in the energy dependence of Q_l and σ_A. One should note that as quasi-steady states may lie deep under a potential hump, a more careful procedure of integrating the radial equation is used in this case. It is based on the treatment presented in [24] and consists of a construction of two linearly independent solutions $z_\pm$ of the radial equation in the classically forbidden region under the hump. z_+ is an increasing function of r, z_--decreasing. These solutions are calclulated by the numerical integration in directions of their growth. The radial function in the relevant region is a linear combination of $z_\pm$ with coefficients $A_\pm$ which are found by its join with the function obtained at less r. Thus, the radial function becomes known under the hump. Then the numerical integration continues to the asymptotic region where the phase shift is determined. Peaks in Q_l appear near energies at which the coefficient A_+ vanishes. By localizing a zero of A_+ and studying its vicinity with a smaller and smaller energy step it is possible to establish the shape of the corresponding peak.

After the phase shifts have been found, the relevant cross-sections are calculated by the direct summation of partial waves in (12−15). As δ_l follows the power law (19) at large l, a rather large number of waves has to be taken into account. Especially slow is the convergence of the series of $\mathrm{Re}f(\vartheta)$. Even outside a small-angle region a few thousands of terms have to be taken to provide an accuracy of 10^{-3}. Some plots of the elastic differential cross-section *vs.* the center-of-mass scattering angle ϑ are shown in Figures 5-7. Presented also, are classical differential cross-sections calculated with the help of the deflection functions plotted in Figures 2 and 3. Again a number of peculiar features is observed. At small ϑ the quantum cross-section has a peak of a finite height which becomes sharper and sharper as the collision energy is increased. It is due to the scattering by the long-range potential tail (8). The classical cross-section is, of course, infinite at $\vartheta = 0$. Outside a small-angle region the quantum cross-section shows slow oscillations on which rapid ones are superimposed. Such a behaviour is known to be typical for potentials with an inner repulsion and an outer attraction [23]. Such a potential allows a few paths having different impact parameters but scattered at one and the same angle. In the simplest case to which Figures 6 and 7 relate, the collision energy is so large that the orbiting phenomenon is impossible and the classical deflection function has the minimum of a depth $\vartheta_l < \pi$ (Fig. 3). Accordingly, there are three paths scattered at an angle $\vartheta < \vartheta_r$. Two of them specified by the condition $\theta_l = -\vartheta$ lie mostly in the outer attraction region. The interference of their contributions to the scattering amplitude gives rise to the slow

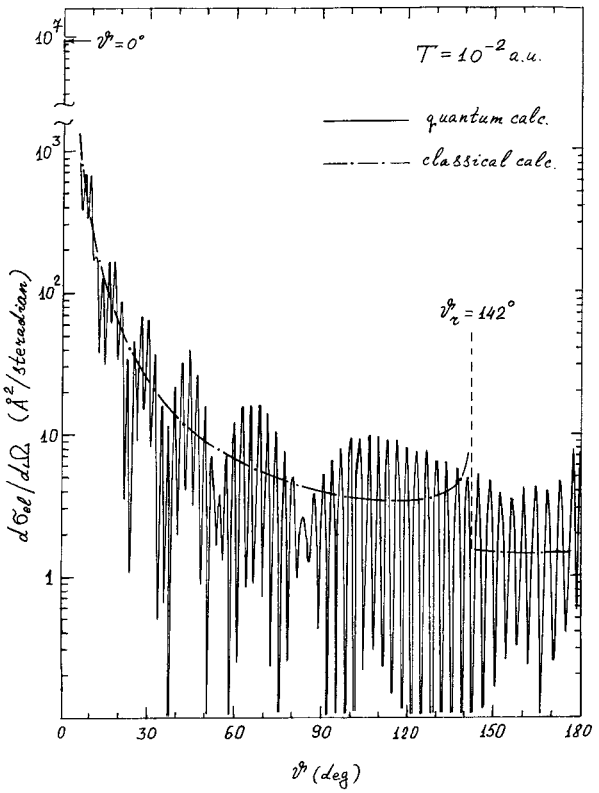

Fig. 6. The elastic differential cross-section *versus* the center-of-mass scattering angle for the rainbow scattering at $T = 10^{-2}$. The horizontal arrow indicates the quantum cross-section at $\vartheta = 0°$.

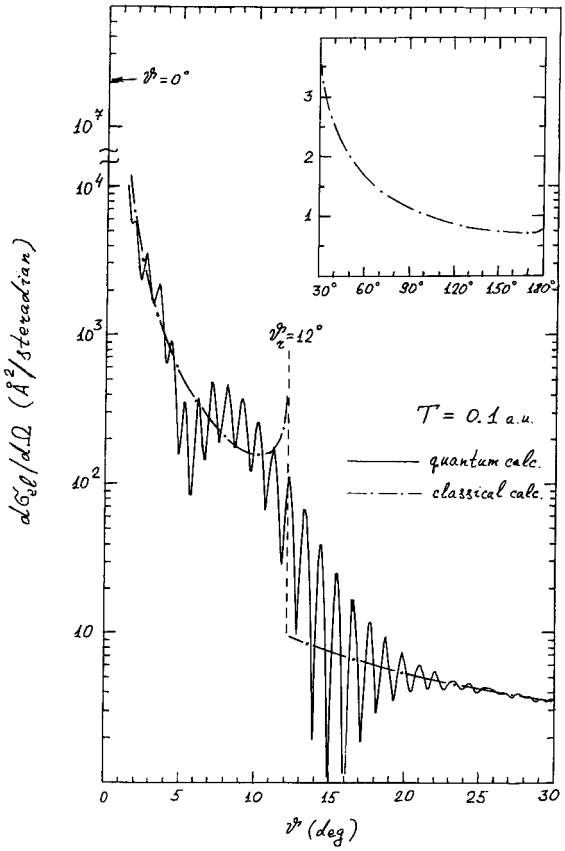

Fig. 7. The elastic differential cross-section *versus* the center-of-mass scattering angle for the rainbow scattering at $T = 10^{-1}$. In the insert is shown the classical cross-section at $30° \leq \vartheta \leq 180°$. The quantum cross-section is very close to this curve.

oscillations. The third path for which $\theta_l = \vartheta$ penetrates into the repulsion region. The addition of its contribution causes the rapid oscillations. In the vicinity of ϑ_r the behaviour peculiar to the rainbow scattering is observed. As ϑ migrates to the region $\vartheta > \vartheta_r$, the slow oscillations disappear at first, then the rapid ones die gradually, and the quantum cross-section becomes nearer and nearer to the classical one. At such angles the latter is contributed only by one path, while at $\vartheta < \vartheta_r$ the three paths contribute and the classical cross-section has a singularity at $\vartheta \to \vartheta_r$ from the left. As the collision energy T is increased, the rainbow scattering angle ϑ_r decreases nearly as T^{-1}. As a result, appreciable differences between the quantum and classical cross-sections migrate to the small-angle region. It is interesting to note that the two kinds of oscillations of the quantum cross-section exist also at lower energies when the orbiting phenomenon occurs (Fig. 5). In this case an infinite number of paths are scattered at any angle ϑ. It is convenient to distinguish two families of such paths according to values of the deflection function:

$$\theta_l = \pm\vartheta - 2\pi n_\pm, \tag{20}$$

$n_\pm$ are non-negative integers indicating how many complete revolutions about the scattering center a path makes. Two attractive paths encircling the center at different distances correspond to each $n_\pm$, except $n_+ = 0$ for which a single repulsive path exists. Both the initial and final asymptotic branches of the paths of the plus-family lie on one side of the center. For the paths of the minus-family they are on different sides. The classical differential cross-section is a sum of an infinite series which, however, converges rather fast (like a geometric progression). At $\vartheta \leq 90°$ the main contribution comes from three paths with minimum values of $\theta_l(n_\pm = 0)$. It appears the interference of scattering amplitudes corresponding to these paths gives rise to the oscillations of the quantum cross-section, similar to the case of higher energies. As ϑ is increased, attractive paths with $n_+ = 1$ become more and more significant, but the situation is not changed qualitatively and the oscillations remain. However, because of attractive paths the classical cross-section becomes infinite at $\vartheta \to 180°$ unlike the cases shown in Figures 6 and 7. The quantum cross-section remains, of course, finite in this limit.

Shown in Figure 8 are plots of the total elastic σ_{el} and reaction σ_A cross-sections *vs.* the collision energy T. Moreover, presented are the diffusion cross-section σ_d and the mean energy loss $\langle\varepsilon\rangle$ of $(\mu\mathrm{B})^{4+}$ in an individual elastic collision. σ_d is defined by

$$\sigma_d = \int (1 - \cos\vartheta)(d\sigma_{el}/d\Omega)d\Omega. \tag{21}$$

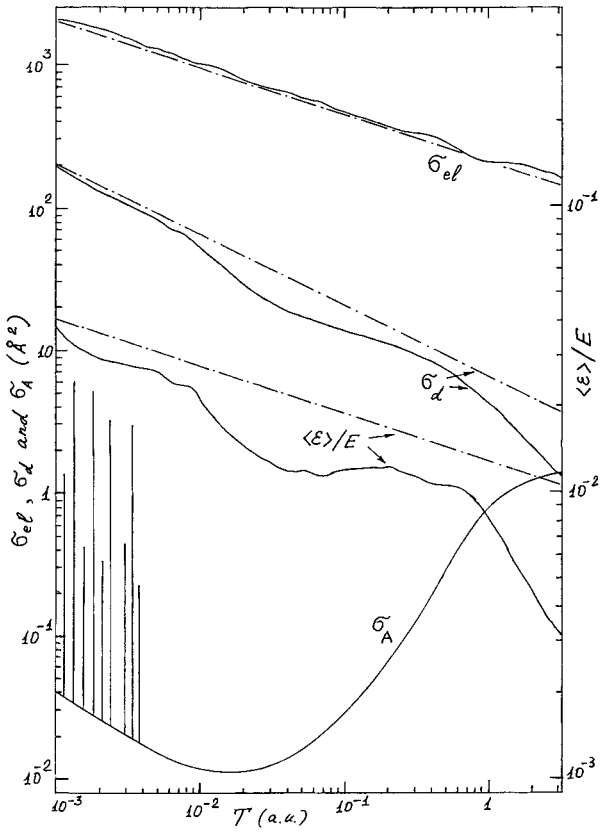

Fig. 8. The total elastic σ_{el}, diffusion σ_d and reaction σ_A cross- sections (left ordinates) as well as the mean energy loss $\langle\varepsilon\rangle$ divided by the μ-atom energy E (right ordinates) *versus* the collision energy T. The solid curves are results of the "exact" calculation, the dash-dot ones are obtained with the simplified formulae (26-27).

The integration is carried out analytically with the help of (12) and properties of Legendre polynomials. The resulting expression is an infinite series in terms of δ_l and μ_l. $\langle\varepsilon\rangle$ is connected with σ_d and σ_{el}. Let E and $(E-\varepsilon)$ be the energies of $(\mu\mathrm{B})^{4+}$ before and after an elastic collision. They are specified in the laboratory frame where helium atoms are treated as if at rest. The relation of E to the collision energy T is:

$$E = \left(\frac{m_{\mu\mathrm{B}}}{m}\right) T \approx 3.5T. \tag{22}$$

$m_{\mu\mathrm{B}}$ is the mass of $(\mu\mathrm{B})^{4+}$. The energy loss ε is expressed in terms of the center-of-mass scattering angle ϑ by

$$\varepsilon = (2m/M)E(1-\cos\vartheta). \tag{23}$$

M is the total mass of $(\mu\mathrm{B})^{4+}$ and He^{2+}. The mean energy loss is:

$$\langle\varepsilon\rangle = {\sigma_{el}}^{-1} \int \varepsilon(d\sigma_{el}/d\Omega)d\Omega. \tag{24}$$

It is clear that

$$\langle\varepsilon\rangle = (2m/M)E(\sigma_d/\sigma_{el}). \tag{25}$$

In Figure 8 shown also are energy dependences of σ_{el}, σ_d and $\langle\varepsilon\rangle$ obtained within some simplifying assumptions. In the series (14) all μ_l are taken to be equal to zero, $\cos 2\delta_l$ is treated to be a random function at l less than some l_0 and the Born approximation (19) is used at $l \geq l_0$. l_0 is determined from the condition $\theta_{l_0} = 1$. The corresponding result is [20]:

$$\sigma_{el} = 4\pi[2(\pi\beta)^2 m/T]^{1/3}. \tag{26}$$

A similar method applied to σ_d yields [25]:

$$\sigma_d = 2.12\pi(8\beta/T)^{1/2}. \tag{27}$$

The approximation for $\langle\varepsilon\rangle$ follows from (25-27). In a log-log scale these dependences are linear. It is known [26,27] that the presence of maxima in δ_l (Figs. 2,3) contradicts the assumption of a random nature of $\cos 2\delta_l$ and leads to undulations of the σ_{el} and σ_d curves. It is seen from Figure 8 that the "exact" σ_{el} curve is near the straight line specified by (26) and an amplitude of its undulations is small. These mean that the δ_l maxima do not play any significant role in σ_{el}. This is quite clear because a considerable contribution to σ_{el} comes from high l waves scattered by the long-range attractive potential tail (8). For the same reason $d\sigma_{el}/d\Omega$ is sharply peaked forward and σ_{el} is very large-right up to 2×10^3 Å^2 at low energies. More appreciable are manifestations of the δ_l maxima in σ_d and $\langle\varepsilon\rangle$. This is due to the contribution of high l waves (or, equivalently, that of small scattering angles) being suppressed in the corresponding formulae. Such a suppression results also in the inequalities $\sigma_d \ll \sigma_{el}$ and $\langle\varepsilon\rangle \ll E$. Thus, small-angle elastic scattering with small energy losses predominates. It is interesting to note that the energy loss distribution has an appreciable dispersion. It is specified by the mean square of the energy loss $\langle\varepsilon\rangle^2$ whose definition differs from (24) by the power of ε in the integrand. Finally $\langle\varepsilon^2\rangle$ is also expressed in terms of δ_l and μ_l. The calculation indicates that at all the relevant energies $\langle\varepsilon^2\rangle^{1/2}$ is greater than $\langle\varepsilon\rangle$ by a factor of 4−6, and its energy dependence also shows appreciable undulations caused by the δ_l maxima. We do not present the corresponding curve because $\langle\varepsilon^2\rangle$ will be unnecessary later on.

Concerning the reaction cross-section σ_A, its energy dependence shown in Figure 8 is, in general outline, similar to that calculated in [19]. As before, at $T \leq 10^{-2}$ the smooth curve is approximately described by the v^{-1} law. Some increase of σ_A in this region compared to [19] is due to the more accurate definition of $U(r)$. However, as was already mentioned, the present quantum-mechanical consideration predicts sharp peaks in σ_A at low energies. The most intensive of them are shown in Figure 8. Some peaks are seen to reach a few Å^2 which exceeds nonpeak values typical for the given energy region by two orders of magnitude. However, as these peaks are connected with quasi-steady states lying deep under a potential hump, their widths are very small-of the order of 10^{-4} or 10^{-5} of their energies. One should note that resonance features appear also on the other solid curves plotted in Figure 8. This is due to some terms in the corresponding partial-wave

expansions passing through an extremum. For σ_{el} such features are insignificant. Their amplitudes do not exceed a few per cent. This results from σ_{el} being contributed by a much greater number of waves than σ_A. More appreciable are deviations of σ_d from its smooth curve which are of 20−30%. Such an increase compared to σ_{el} is due to the suppression of the high l waves contribution. As the behaviour of σ_{el} and σ_d at near-thermal energies where the resonance features are localized is unnecessary for the subsequent consideration, we do not examine these features in detail and do not show them in Figure 8. One should also make a remark concerning the mass dependence of the relevant cross-sections. In the previous analysis the mass of $(\mu^{10}\mathrm{B})^{4+}$ was used. The use of those of $\mu^{11}\mathrm{B}$ or the actual isotope ^{9}Be leads to insignificant (a few per cent) changes of σ_{el}, σ_d and σ_A. Finer features similar to extrema in $d\sigma_{el}/d\Omega$ or peaks in σ_A are, of course, more sensitive. However, they will also be unnecessary later on.

3 A migration kinetics of $(\mu\mathrm{B})^{4+}$ in helium and the two-photon decay of the 2s state

Let $(\mu\mathrm{B})^{4+}$ in its $2s$ state be formed in helium with a small admixture of diborane so that the inequality (5) is satisfied and only collisions of $[\mu\mathrm{B}(2s)]^{4+}$ with helium atoms are significant. Let us consider how these collisions effect the two-photon $2s \to 1s$ transition. We take it that this transition does occur in $[\mu\mathrm{B}(2s)]^{4+}$ but becomes impossible after the μ-atom has intercepted an electron in the reaction (4) [1]. Helium is treated as an infinite, homogeneous medium. This approximation seems to be reasonable because typical paths of $[\mu\mathrm{B}(2s)]^{4+}$ during its lifetime (32 ns) are small compared to the size of a muon stop volume in the experiment [18]. For instance, even without collisions the path of the μ-atom with the energy $E = 1$ is about 1 mm while the stop volume is of a few cm. For the same reason we do not consider the space distribution of two-photon decays which is mainly determined by that of muon stops. In such a situation the migration of muonic boron in helium is described by a distribution function $f(E,t)$ defined so that $f(E,t)dE$ is the probability that at a moment t the laboratory-frame energy of $[\mu\mathrm{B}(2s)]^{4+}$ lies between E and $(E+dE)$. Any quantity concerning the $2s$ state decay can be expressed in terms of this function. For instance, the probability of $[\mu\mathrm{B}(2s)]^{4+}$ having lived till the moment t is:

$$P_{2s}(t) = \int_0^\infty f(E,t)dE. \tag{28}$$

As the formation of muonic boron takes a time much shorter than the $2s$ state lifetime, it is natural to consider that $[\mu\mathrm{B}(2s)]^{4+}$ arises instantly at $t = 0$. Accordingly,

$$P_{2s}(t=0) = 1. \tag{29}$$

[1] Actually, the two-photon transition yield is about 98.5% for $(\mu\mathrm{B})^{4+}$ [9] and about 3% for the μ-atom with one K-electron [12]. In the latter case the main decay modes are the $2s \to 1s$ transitions with emission of either one hard electron (about 60%) or a hard photon and a soft electron.

Let also $P_{2\gamma}(t)$ and $P_e(t)$ be respectively the probabilities of the two-photon transition and the electron transfer (4) within the time t. It is clear that

$$dP_{2\gamma}/dt = \lambda_{2\gamma} P_{2s}(t), \tag{30}$$

$$dP_e/dt = \gamma(t) \equiv \int_0^\infty \lambda_A(E) f(E,t) dE, \tag{31}$$

$$\lambda_A(E) = \rho_{\mathrm{He}} v(E) \sigma_A(E). \tag{32}$$

$\lambda_{2\gamma}$ and ρ_{He} were introduced in (1), $v(E)$ is the velocity of the μ-atom with the energy E, $\sigma_A(E)$ is the cross-section of (4). As $P_{2\gamma}$ and P_e vanish at $t = 0$, we have:

$$P_{2\gamma}(t) = \lambda_{2\gamma} \int_0^t P_{2s}(t')dt', \tag{33}$$

$$P_e(t) = \int_0^t \gamma(t')dt'. \tag{34}$$

The yield of the two-photon transition introduced in (1) is

$$Y_{2\gamma} = P_{2\gamma}(t \to \infty). \tag{35}$$

Analogously defined is the yield of the electron transfer

$$Y_e = P_e(t \to \infty). \tag{36}$$

$P_{2s}(t)$ vanishes in this limit.

The function $f(E,t)$ obeys a kinetic equation which is easily constructed by writing the balance of μ-atoms in a volume $dEdt$. This yields:

$$\partial f(E,t)/\partial t = -\lambda(E) f(E,t) - \rho_{\mathrm{He}} v(E) \sigma_{el}(E) f(E,t) + \rho_{\mathrm{He}} \int_0^\infty d\varepsilon \frac{d\sigma_{el}(E';\varepsilon)}{d\varepsilon} v(E') f(E',t)\Big|_{E'=E+\varepsilon}. \tag{37}$$

The first term on the right describes quenching the $2s$ state due to the two-photon transition and the electron transfer. $\lambda(E)$ is the quenching rate:

$$\lambda(E) = \lambda_{2\gamma} + \lambda_A(E). \tag{38}$$

The two other terms correspond to μ-atoms leaving and filling the interval $(E,\ E + dE)$ due to elastic collisions. $d\sigma_{el}(E' = E + \varepsilon;\varepsilon)/d\varepsilon$ is the cross-section of the elastic collision in which the energy of $[\mu\mathrm{B}(2s)]^{4+}$ is decreased from E' to E; ε is the energy loss. A simple relation of this cross-section to $d\sigma_{el}/d\Omega$ follows from (23):

$$d\sigma_{el}(E';\varepsilon)/d\varepsilon = (M/m)(\pi/E')d\sigma_{el}/d\Omega. \tag{39}$$

With the help of (37) it is easy to check that at any $t \geq 0$ the following obvious relation is valid:

$$P_{2s}(t) + P_{2\gamma}(t) + P_e(t) = 1. \tag{40}$$

In the limit $t \to \infty$ it yields

$$Y_{2\gamma} + Y_e = 1. \tag{41}$$

To determine the function $f(E,t)$ it is necessary to solve the equation (36) with an initial condition

$$f(E, t=0) = f_0(E). \tag{42}$$

$f_0(E)$ is to satisfy (29). It is clear that this procedure is very complicated. To avoid it we simplify (37) by making use of the so-called "continuous loss approximation" which is often employed in problems associated with the passage of heavy charged particles through a medium [28]. It is based on the already-mentioned fact that typical energy losses in individual elastic collisions are small ($\langle\varepsilon\rangle \ll E$). This allows the integrand of (37) to be replaced by two terms of its expansion in powers of (ε/E):

$$\frac{d\sigma_{el}(E';\varepsilon)}{d\varepsilon} v(E') f(E',t) \cong \frac{d\sigma_{el}(E;\varepsilon)}{d\varepsilon} v(E) f(E,t) + \varepsilon \frac{\partial}{\partial E}\left[\frac{d\sigma_{el}(E;\varepsilon)}{d\varepsilon} v(E) f(E,t)\right]. \tag{43}$$

As a result, the integro-differential equation (37) is transformed into the partial differential equation

$$\partial f(E,t)/\partial t = -\lambda(E) f(E,t) + \partial[\varphi(E) f(E,t)]/\partial E, \tag{44}$$

$$\varphi(E) = \rho_{\mathrm{He}} v(E) \sigma_{el}(E) \langle\varepsilon(E)\rangle. \tag{45}$$

$\langle\varepsilon(E)\rangle$ is the mean energy loss given by (25). It is obvious that $\varphi(E)$ is actually proportional to the diffusion cross-section σ_d. The equation (44) can be easily solved. As the function $f_0(E)$ involved in the initial condition (42) is now unknown, we limit ourselves to its simplest form:

$$f_0(E) = \delta(E - E_0) \tag{46}$$

E_0 is the initial energy of $[\mu\mathrm{B}(2s)]^{4+}$ which is treated as a parameter. In this case the solution of (44) is written in the form:

$$f(E,t) = \delta(E - E_t) P_{2s}(t), \tag{47}$$

where E_t is defined by the equation

$$t = \int_{E_t}^{E_0} dE'/\varphi(E'), \tag{48}$$

and the probability $P_{2s}(t)$ is:

$$P_{2s}(t) = \exp(-\lambda_{2\gamma} t) \exp\left[-\int_{E_t}^{E_0} \lambda_A(E') \varphi^{-1}(E') dE'\right]. \tag{49}$$

The form (47) allows the expression (34) to be simplified:

$$P_e(t) = \int_0^t \lambda_A(E_{t'}) P_{2s}(t') dt'. \tag{50}$$

$E_{t'}$ and t' are related similarly to (48). For $P_{2\gamma}(t)$ the formula (33) is still convenient.

Let us discuss the obtained results. The function (47) is seen to correspond to an ensemble of monoenergetic μ-atoms. E_t is their energy at the moment t. This result indicates a limitation of the present model which can not describe spreading the initial energy distribution (46) caused by energy loss fluctuations in individual elastic collisions [28]. For this reason the derived formulae may be applied only at sufficiently high energies when the energy distribution of μ-atoms has not yet been too distorted compared to the initial one. A consideration of spreading needs, at least, to take into account the term quadratic in (ε/E) in the expansion (43). As a consequence, one more term appears on the right of (44). It involves the second derivative with respect to E as well as $\langle\varepsilon^2\rangle$. The resulting equation is unlikely to be solvable in quadratures because of complicated energy dependences of its coefficients. Additional complications arise at near-thermal E when the motion of helium atoms has to be taken into account in (37). An alternative means of consideration may be based on a Monte-Carlo method. However, before that it is necessary to construct smoothed analytical approximations of the angular distributions $d\sigma_{el}/d\Omega$. In either case a more realistic consideration of $f(E,t)$ needs serious additional work which has not been carried out here.

In Figures 9 and 10 are plotted the probabilities $P_{2\gamma}$ and P_e as well as the energy E_t *vs.* the time t. The plots were made with the help of the above-presented formulae at several initial energies E_0 and helium pressures P_{He}. The temperature was taken to be equal to 300 K. The cross-sections calculated in Section 2 were used in a numerical evaluation of the relevant integrals. Let us note some features of the presented curves. The time dependences of E_t prove to be nearexponential. This can be easily realized on the basis of the approximation (27) within which $\varphi(E) \propto E^{-1}$ and E_t is:

$$E_t = E_0 \exp(-t/\tau_E), \tag{51}$$

$$\tau_E = (\rho_{\mathrm{He}} \chi)^{-1}, \tag{52}$$

$$\chi = 16.96\pi(\beta m)^{1/2} M^{-1}. \tag{53}$$

However, as the cross-section σ_d found with (27) is greater than that obtained by the numerical calculation (Fig. 8), the formula (51) predicts a faster moderation. Concerning the electron transfer probability P_e, it increases first with t and then tends to a saturation. Such a behaviour can be explained in the following way. The slope dP_e/dt is seen from (50) to be equal to the product $\lambda_A(E_t) P_{2s}(t)$. Both the multipliers decrease with t and the slope decreases also. Physically this means that the electron transfer occurs mostly at an initial stage of the moderation when P_{2s} is not yet too small and E is still sufficiently high for $\lambda_A(E)$ to be an appreciable part of the total quenching rate $\lambda(E)$. The latter circumstance leads also to the saturation becoming more and more distinct as E_0 is increased. One may construct a simple model clarifying the

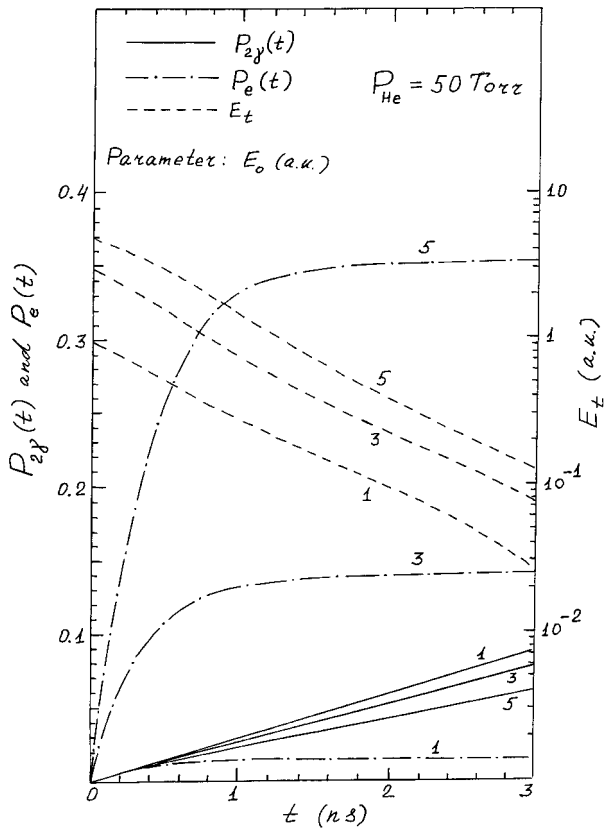

Fig. 9. The probabilities of the two-photon transition $P_{2\gamma}$ and the electron transfer P_e (left ordinates) as well as the μ-atom energy E_t (right ordinates) *versus* the time t at the helium pressure $P_{\rm He} = 50$ Torr.

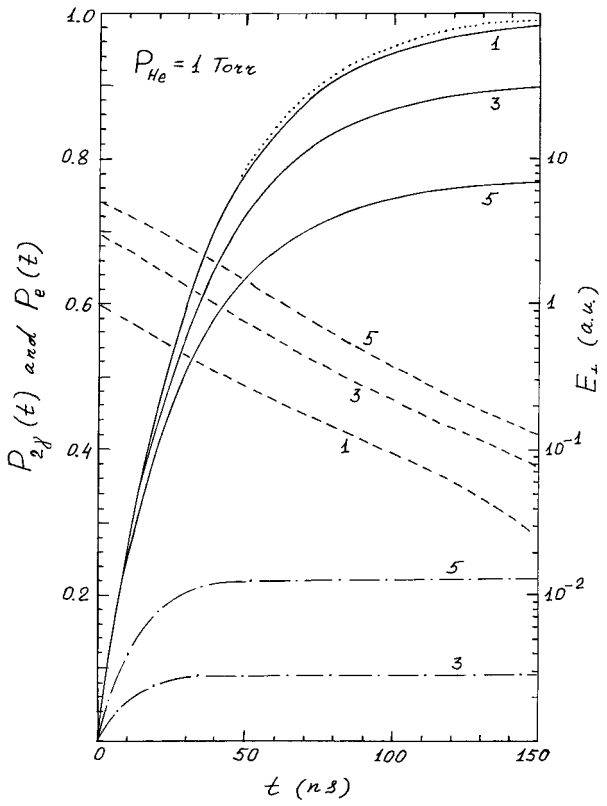

Fig. 10. The probabilities $P_{2\gamma}$ and P_e as well as the energy E_t *versus* the time t at the helium pressure $P_{\rm He} = 1$ Torr. The notation is similar to that of Figure 9. The P_e curve for $E_0 = 1$ is not given because it is very near the horizontal axis. The dotted curve shows the time dependence of $P_{2\gamma}$ for an isolated $[\mu{\rm B}(2s)]^{4+}$.

time dependence of P_e. It is based on the approximation (27) and on the assumption that the reaction cross-section σ_A is an energy-independent constant. The latter is reasonable at $E \geq 3.5$ ($T \geq 1$ in Fig. 8). In this case the integral involved in (49) is easily taken and P_{2s} is:

$$P_{2s}(t) = \exp(-\lambda_{2\gamma} t) \exp[-\alpha(E_0^{1/2} - E_t^{1/2})], \qquad (54)$$

$$\alpha = \sigma_A (8/m_{\mu{\rm B}})^{1/2} \chi^{-1}. \qquad (55)$$

E_t is given by (51). P_e can be expressed in a simple form at

$$t \ll {\lambda_{2\gamma}}^{-1} \approx 32 \text{ ns}, \qquad (56)$$

when the first exponent in (54) may be replaced by unity. We have from (50):

$$P_e(t) = 1 - \exp[-\alpha(E_0^{1/2} - E_t^{1/2}], \qquad (57)$$

If, in addition to (56), t obeys the inequality

$$\tau_E \ll t, \qquad (58)$$

E_t becomes much less than E_0 and both P_{2s} and P_e take constant values:

$$P_{2s} = \exp(-\alpha E_0^{1/2}), \qquad (59)$$

$$P_e = 1 - \exp(-\alpha E_0^{1/2}). \qquad (60)$$

This clearly indicates the saturation of P_e. The obtained formulae are applicable at pressures sufficiently high for the inequalities (56) and (58) to be compatible. In particular, such a situation is shown in Figure 9 where τ_E is about 0.6 ns. In this case the expression (60) accounts qualitatively for some features of the "exact" P_e curves. For instance, in accordance with (52) a typical duration of the presaturation stage varies inversely with $P_{\rm He}$ and depends weakly on E_0. The saturation value is much more sensitive to E_0 than to $P_{\rm He}$ in agreement with (60). The expressions (59) and (60) are valid to the zeroth order in the small parameter

$$\lambda_{2\gamma} \tau_E \ll 1. \qquad (61)$$

Their sum being equal to unity means that the two-photon transition probability $P_{2\gamma}$ vanishes in this order. Indeed, from (33) it is clear that $P_{2\gamma}$ is linear in the parameter (61). As a result, during the presaturation stage $P_{2\gamma}$ proves to be appreciably less than P_e. This inequality is emphasized as $P_{\rm He}$ and E_0 are increased (Fig. 9). The two-photon transition occurs mostly after the saturation has come. At this stage the electron transfer is already insignificant ($\lambda_A \ll \lambda_{2\gamma}$) and the remaining $[\mu{\rm B}(2s)]^{4+}$ are

quenched by the exponential decay law with the constant $\lambda_{2\gamma}$. In particular, within the above-presented simplified model the yields $Y_{2\gamma}$ and Y_e are obviously equal to (59) and (60) respectively. As the pressure is decreased, the product $(\lambda_{2\gamma}\tau_E)$ becomes comparable with unity. Such a case is shown in Figure 10. The electron transfer and the two-photon transition are not separated in time and occur in parallel. For this reason at a fixed E_0 the saturation value of P_e decreases compared to the case (61) and $Y_{2\gamma}$ increases. It is of interest to compare quantitative predictions of the time dependence of P_e obtainable from (57) with those based on the numerical calculation. The parameter σ_A involved in (55) is found by equating the "exact" saturation value to (60). To avoid an excess of Figures we do not present curves obtained in this way. Actually they are consistently lower than the "exact" curves. This is due to a faster moderation predicted by (51). In particular, σ_A proves to be several times less than values expected on the basis of the $\sigma_A(T)$ curve shown in Figure 8.

It was already mentioned that the results (47-50) were inapplicable at the final moderation stage when the energy distribution of μ-atoms becomes close to the Maxwellian one. To take into account contributions of this stage to $Y_{2\gamma}$ and Y_e we make use of the fact that at $T \leq 10^{-2}(E \leq 3.5\times 10^{-2})$ the nonresonance part of the cross-section $\sigma_A(T)$ varies approximately in inverse proportion to the relative velocity v:

$$\sigma_A(T) = \kappa v^{-1}, \tag{62}$$

$\kappa \approx 5.5 \times 10^{-13}$ cm^3 s^{-1} [2]. Let us rewrite (31) in a more general form:

$$dP_e/dt = \rho_{\mathrm{He}}\xi(t)P_{2s}(t), \tag{63}$$

$$\xi(t) = \langle v\sigma_A(T)\rangle P_{2s}^{-1}(t). \tag{64}$$

The brackets in (64) mean averaging over the function $f(E,t)$ and, in addition to (31), over the Maxwellian distribution of helium atoms. The presence of P_{2s} in such an artificial form is connected with the normalization (28). It allows $\xi(t)$ to be treated as a reaction rate constant. At the final stage of the moderation the function $f(E,t)$ is nonvanishing at energies for which the approximation (62) is valid. In this case $\xi(t)$ is:

$$\xi(t) = \kappa + \xi_p(t). \tag{65}$$

The first term results from (62), the second term is contributed by the peaks existing in $\sigma_A(T)$ at thermal energies (Fig. 8). The ratio of these terms may be estimated in the following way:

$$\xi_p(t)/\kappa \sim 10^2 \times 10^{-4} = 10^{-2} \ll 1. \tag{66}$$

The first multiplier 10^2 is a typical factor by which peak values of σ_A exceed nonpeak ones, the second multiplier 10^{-4} is a typical ratio of a peak width to the temperature. Thus, because of the narrowness of the peaks their contribution to (65) proves to be negligible and the reaction rate constant may be considered to be time-independent: $\xi(t) = \kappa$. Then a simple differential equation for $P_{2s}(t)$ is obtained from (30), (40), and (63). Its solution is:

$$P_{2s}(t) = P_{2s}(t_0)\exp[-\lambda_0(t-t_0)]. \tag{67}$$

$$\lambda_0 = \lambda_{2\gamma} + \rho_{\mathrm{He}}\kappa. \tag{68}$$

t_0 is a moment after which the approximation (62) may be used. We assume that the "continuous loss approximation" is valid right up to this moment and determine it with the formula (48) in which the lower limit $E_t = 3.5 \times 10^{-2}$ (this energy exceeds typical thermal values by a factor of 20−30). $P_{2s}(t_0)$ is found with (49). The substitution of (67) in (30) and (63) yields for $t \geq t_0$:

$$P_{2\gamma}(t) = (\lambda_{2\gamma}/\lambda_0)P_{2s}(t_0)\{1 - \exp[-\lambda_0(t-t_0)]\}, \tag{69}$$

$$P_e(t) = (\rho_{\mathrm{He}}\kappa/\lambda_0)P_{2s}(t_0)\{1 - \exp[-\lambda_0(t-t_0)]\}. \tag{70}$$

In the limit $t \to \infty$ these formulae yield the contributions of the final moderation stage to $Y_{2\gamma}$ and Y_e. Finally we have:

$$Y_{2\gamma} = P_{2\gamma}(t_0) + (\lambda_{2\gamma}/\lambda_0)P_{2s}(t_0), \tag{71}$$

$$Y_e = P_e(t_0) + (\rho_{\mathrm{He}}\kappa/\lambda_0)P_{2s}(t_0). \tag{72}$$

The terms $P_{2\gamma}(t_0)$ and $P_e(t_0)$ are the contributions of the interval $0 \leq t \leq t_0$. They are found within the "continuous loss approximation" with the formulae (33) and (49-50). It is clear that $Y_{2\gamma}$ and Y_e given by (71-72) obey (41).

Plots of $(Y_{2\gamma})^{-1}$ *vs.* the helium pressure made for several E_0 are shown in Figure 11. The use of $(Y_{2\gamma})^{-1}$ is convenient because in this case the dependence (1) with $\rho_{\mathrm{B_2H_6}} = 0$ is represented by a straight line:

$$(Y_{2\gamma})^{-1} = 1 + \rho_{\mathrm{He}}(q_{\mathrm{He}}/\lambda_{2\gamma}). \tag{73}$$

The plots of Figure 11 are seen to look more complicated. They become straight-line provided P_{He} exceeds some value increasing with E_0. For such pressures we have:

$$(Y_{2\gamma})^{-1} = C(1 + \rho_{\mathrm{He}}D). \tag{74}$$

The plot of C *vs.* E_0 is also shown in Figure 11. Unlike (73), C proves to be greater than unity and increases fast with E_0. This can be realized on the basis of the consideration undertaken in connection with (51-61). As P_{He} is increased, the following inequalities become valid:

$$\lambda_{2\gamma}t_0 \ll 1, \tag{75}$$

$$P_{2\gamma}(t_0) \ll P_{2s}(t_0). \tag{76}$$

Under the condition (75) the moderation to near-thermal energies is very fast so that the electron transfer and

[2] κ may be increased by a factor of 1.5−2 because of uncertainties of the calculation of the Auger decay rate $W(r)$ at large r [19].

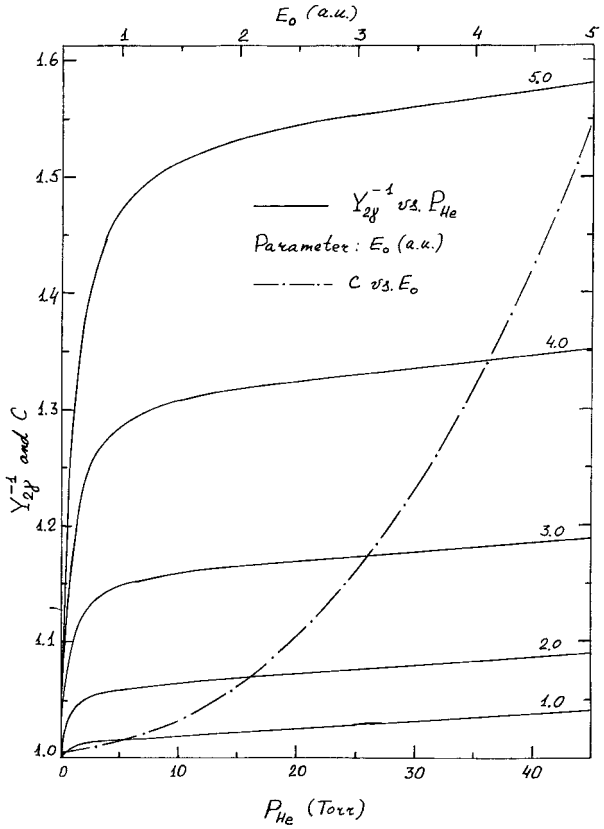

Fig. 11. The inverse two-photon transition yield $(Y_{2\gamma})^{-1}$ *versus* the helium pressure $P_{\rm He}$ and the factor C *versus* the initial energy of muonic boron E_0 (upper abscissae).

the two-photon transition are separated in time. The former occurs mostly during the moderation while the latter is responsible for the decay of $[\mu{\rm B}(2s)]^{4+}$ remaining unquenched by the moderation's end. Accordingly, the first term in (71) may be neglected and $(Y_{2\gamma})^{-1}$ takes the form

$$(Y_{2\gamma})^{-1} = [P_{2s}(t_0)]^{-1}[1 + \rho_{\rm He}(\kappa/\lambda_{2\gamma})]. \qquad (77)$$

The comparison with (74) yields:

$$C = [P_{2s}(t_0)]^{-1}, \qquad (78)$$

$$D = \kappa/\lambda_{2\gamma}. \qquad (79)$$

In the limit (75), $P_{2s}(t_0)$ depends solely on E_0 and decreases with it (see Eq. (59)). Accordingly, C increases near-exponentially.

The previous consideration clearly indicates the information which may be extracted from measurements of $Y_{2\gamma}$. Let us assume that the dependence of $(Y_{2\gamma})^{-1}$ on $P_{\rm He}$ has been found in an experiment performed under the condition (5), and that it shows the straight-line branch. Its fit yields the factors C and D. The plot of C *vs.* E_0 shown in Figure 11 allows a typical value of E_0 to be estimated. In particular, an appreciable deviation of C from unity may be an indicator of an additional acceleration of muonic boron during its formation in the diborane molecule (caused, for instance, by its Coulomb repulsion from positively charged molecular fragments). Moreover, in this case it is possible to estimate the probability $P_{2s}(t_0)$ of the unquenching of $[\mu{\rm B}(2s)]^{4+}$ during its moderation to near-thermal energies as well as the probability $P_e(t_0)$ of the electron transfer at this stage. The former is obtained from (78), the latter-from the equality

$$P_{2s}(t_0) + P_e(t_0) = 1, \qquad (80)$$

which is valid at sufficiently large E_0 in the limit (75). Concerning the factor D, it allows the rate constant κ of the electron transfer at low energies to be determined. In particular, if C is close to unity, the form (74) is identical to (73) which is the extrapolation of (1) to vanishing $\rho_{\rm B_2H_6}$. In this case $q_{\rm He}$ coincides with κ. The theoretical value of κ presented in (62) is seen to lie within the experimental interval (2).

The results obtained in this section relate to an idealized case in which the partial pressure of diborane is so small that its contribution to the electron transfer is negligible. The lowest diborane pressure achieved in the experiment [18] is not yet sufficient for such a situation to occur. In this case the electron transfer is still due to collisions of muonic boron with diborane molecules. As the corresponding cross-section is now unknown, any quantitative predictions are impossible. However, some remarks of a qualitative kind can be made based on the results of the present work. For instance, by analogy to (74) it is possible to suggest the following formula to fit the data of [18]:

$$(Y_{2\gamma})^{-1} = C'[1 + \rho_{\rm He}(q_{\rm He}/\lambda_{2\gamma}) + \rho_{\rm B_2H_6}(q_{\rm B_2H_6}/\lambda_{2\gamma})]. \qquad (81)$$

It differs from (1) by one additional fitted parameter C' similar to C in (74). That C was found to be unequal to unity is due to the v^{-1} law (62) for the reaction cross-section σ_A being valid only within a limited interval of collision energies. Otherwise the rate λ_A (32) is energy-independent, the time dependence of P_{2s} following from (49) is exponential at any form of the function $\varphi(E)$, and the factor C is obtained to be exactly equal to unity. Actually, deviations of σ_A from the v^{-1} law grow fast at $T \geq 10^{-2}$. For this reason the second multiplier in (49) responsible for a nonexponential decay of the $2s$ state increases with E_0, and C increases too. In the case of the experiment [18], σ_A is replaced by the total cross-section σ_t of the electron transfer from diborane to muonic boron (this transfer is assumed to be the main inelastic channel). If within an interval of relevant collision energies the energy dependence of σ_t deviates considerably from the v^{-1} law, the factor C' may be expected to differ appreciably from unity. Dr. K. Kirch kindly agreed to make a fit of the experimental data with the help of (81). Unfortunately, because of a low statistical accuracy of the data a reliable fixation of C' proved to be impossible.

Finally let us consider why the v^{-1} law may be valid for σ_t and how deviations from it may be interpreted. If the conception of a complex central potential is assumed

to be applicable to describe collisions of muonic boron with diborane molecules, σ_t may be written in the form similar to (15):

$$\sigma_t = (\pi/k^2)\sum_{l=0}^{\infty}(2l+1)X_l. \quad (82)$$

X_l is the total probability of the electron transfer at the given T and l. It is natural to assume that σ_t is mainly contributed by near-central collisions for which l is less than some $l_m \gg 1$. Taking X_l to be a slowly varying function of l at $l \leq l_m$ we obtain:

$$\sigma_t \approx (\pi/k^2)X_{l=0}l_m^2. \quad (83)$$

It is natural to determine l_m from the condition

$$T \geq U_h. \quad (84)$$

U_h is the height of a hump in the effective potential. If the form (8) is taken for the potential, U_h and the hump top radius r_h are:

$$U_h = [l(l+1)]^2/128\beta' m'^2, \quad (85)$$

$$r_h = [32\beta' m'/l(l+1)]^{1/2}. \quad (86)$$

$\beta' = 160.1$ is the polarizability of the diborane molecule [29], m' is the reduced mass of this molecule and μB^{4+}. It follows from (83-85):

$$l_m^2 \approx m'(128\beta' T)^{1/2}, \quad (87)$$

$$\sigma_t \approx 8\pi X_{l=0} v^{-1}(\beta'/m')^{1/2}. \quad (88)$$

These formulae are valid only in a limited energy interval. Indeed, the effective potential has a hump provided

$$r_h \geq r_0. \quad (89)$$

r_0 is a radius at which the long-range attraction (8) disappears. It seems to be of the order of a molecule's size. It is clear from (86) that this inequality becomes invalid as l is increased. The requirement of its validity at $l = l_m$ limits the relative velocity:

$$v \leq 4r_0^{-2}(\beta'/m')^{1/2}. \quad (90)$$

We see from (88) that if the v-dependence of $X_{l=0}$ is weak in the interval (90), σ_t proves to be proportional to v^{-1}. In particular, such a situation takes place for the cross-section σ_A at $T \leq 10^{-2}$. Within the present approach deviations of σ_t from the v^{-1} law result clearly from either apprecible variations of $X_{l=0}$ with v or a violation of the inequality (90). Because of the large diborane polarizability the latter may be expected if the energy of muonic boron E becomes of the order of 0.1.

This work was supported by the Paul Scherrer Institute (PSI). I am very grateful to Drs. L.M. Simons, K. Kirch, P. Hauser, F. Kotmann and D. Taqqu for their hospitality and numerous critical discussions during my stay at PSI.

References

1. J. Bernabeu, T.E.O. Ericson, C. Jarlskog, Phys. Lett. B **50,** 467 (1974).
2. G. Feinberg, M.Y. Chen, Phys. Rev. D **10,** 190 (1974).
3. A.N. Moskalev, JETP Lett. **19,** 216 (1974).
4. J. Missimer, L.M. Simons, Phys. Rep. **118,** 179 (1985).
5. J. Missimer, L.M. Simons, Z. Phys. D **17,** 275 (1990).
6. J. Bernabeu, Nucl. Phys. A **518,** 317 (1990).
7. P. Langacker, Phys. Lett. B **256,** 277 (1991).
8. R. Casalbuoni, S. De Curtis, N. Di Bartolomeo, F. Feruglio, R. Gatto, Nucl. Phys. A **540,** 577 (1992).
9. R. Bacher, Z. Phys. A **315,** 135 (1984).
10. D.P. Grechukhin, A.A. Soldatov, Sov. Phys. JETP **45,** 205 (1977); *Ibidem* **50,** 1039 (1979); Sov. J. Nucl. Phys. **31,** 518 (1980).
11. S.V. Romanov, D.P. Grechukhin, Sov. J. Nucl. Phys. **41,** 623 (1985).
12. D.P. Grechukhin, S.V. Romanov, A.A. Soldatov, Sov. Phys. JETP **62,** 635 (1985); Preprint IAE-4165/1, I.V. Kurchatov Institute of Atomic Energy, Moscow 1985; Sov. J. Nucl. Phys. **43,** 240 (1986).
13. S.V. Romanov, D.P. Grechukhin, Z. Phys. D **22,** 667 (1992); Romanov, S.V.: Z. Phys. D **31,** 219 (1994).
14. G. Carboni, O. Pitzurra, Nuovo Cim. B **25,** 367 (1975).
15. R.O. Mueller, V.W. Hughes, H. Rosenthal, C.S. Wu, Phys.Rev. A **11,** 1175 (1975).
16. J.S. Cohen, J.N. Bardsley, Phys. Rev. A **23,** 46 (1981).
17. L.M. Simons, Phys. Scripta T **22,** 90 (1988).
18. K. Kirch, D. Abbott, B. Bach, P. DeCecco, P. Hauser, D. Horvath, F. Kottmann, J. Missimer, R.T. Siegel, L.M. Simons, D. Viel, Phys. Rev. Lett. **78,** 4363 (1997).
19. S.V. Romanov, Z. Phys. D **41,** 101 (1997).
20. N.F. Mott, H.S.W. Massey, *The Theory of Atomic Collisions*, third edn., *Chap.5, Sect.5; Chap.8, Sect.2; Chap.19 Sect.3* (Clarendon Press, Oxford, 1965).
21. A.A. Radzig, B.M. Smirnov, *Parameters of atoms and atomic ions, Sect. 4.7* (Energoatomizdat, Moscow, 1986, in Russian).
22. K. Smith, *The Calculation of Atomic Collision Processes, Sect. 1.4* (John Wiley & Sons, New York, London, Sydney, Toronto, Inc., 1971).
23. B.H. Bransden, M.R.C. McDowell, *Charge Exchange and the Theory of Ion-Atom Collisions, Chap.2* (Clarendon Press, Oxford, 1992).
24. E. Fermi, *Nuclear Physics, Sect. 3.4* (Chicago University Press, Chicago, 1950).
25. A. Dalgarno, M.R.C. McDowell, A. Williams, Philos. Trans. of the Royal Society of London A **250,** 411 (1958).
26. R.B. Bernstein, J. Chem. Phys. **34,** 361 (1961).
27. D. Beck, *Elastic Scattering of Nonreactive Atomic Systems. In "Molecular Beams and Reaction Kinetics", Proceedings of the International School of Physics "Enrico Fermi"*, edited by Ch. Schlier. (Academic Press, New York, London, 1970).
28. N.P. Kalashnikov, V.S. Remizovich, M.I. Ryazanov, *Collisions of fast charged particles in solids, Sect. 3.2* (Atomizdat, Moscow, 1980, in Russian).
29. H.E. Wirth, E.D. Palmer, J. Phys. Chem. **60,** 911 (1956).